A Miniaturized Platform for Laser Speckle Contrast Imaging

Janaka Senarathna, *Student Member, IEEE*, Kartikeya Murari, *Member, IEEE*, Ralph Etienne-Cummings, *Fellow, IEEE*, and Nitish V. Thakor, *Fellow, IEEE*

***Abstract*—Imaging the brain in animal models enables scientists to unravel new biological insights. Despite critical advancements in recent years, most laboratory imaging techniques comprise of bulky bench top apparatus that require the imaged animals to be anesthetized and immobilized. Thus, animals are imaged in their non-native state severely restricting the scope of behavioral experiments. To address this gap, we report a miniaturized microscope that can be mounted on a rat's head for imaging in awake and unrestrained conditions. The microscope uses laser speckle contrast imaging (LSCI), a high resolution yet wide field imaging modality for imaging blood vessels and perfusion. Design details of both the image formation and acquisition modules are presented. A Monte Carlo simulation was used to estimate the depth of tissue penetration achievable by the imaging system while the produced speckle Airy disc patterns were simulated using Fresnel's diffraction theory. The microscope system weighs only 7 g and occupies less than 5 cm^3 and was successfully used to generate proof of concept LSCI images of rat brain vasculature. We validated the utility of the head-mountable system in an awake rat brain model by confirming no impairment to the rat's native behavior.**

***Index Terms*—Functional imaging, laser speckle contrast imaging, miniaturization.**

I. Introduction

STRUCTURAL and functional imaging of the brain in animal models provides tremendous insights into the underlying biology of neural activity. Together with electrophysiological and neurochemical recordings, it enables scientists to achieve a broader picture of how the brain functions as a system. Conventionally, noninvasive imaging technologies such as functional magnetic resonance imaging and computational tomography have been used for such studies, but they are expensive and elaborate.

Despite these advancements, due to the bulky and heavy nature of the imaging and illumination apparatus, the majority of imaging techniques are performed on anesthetized animals affixed stereotaxically. This greatly restricts the variety and realistic nature of experiments that can be conducted. Furthermore, the effect of drugs used for anesthesia may also play a role in distorting the observed physiological variables [1], [2]. Hence, none of these methods are suitable for long term, chronic recordings and for imaging structure and function in awake and behaving small animals.

Attempts have been made by several groups to alleviate this limitation. Different flavors of fluorescence microscopy such as wide field fluorescence microscopy [3]–[12], confocal microscopy [13] and two photon microscopy [14], [15] have been the focus in a majority of these endeavors. Additionally, Schulz *et al.* [16] reported the approximate miniaturization of a PET system. However, all these methods require the added burden of a contrasting agent as well as requiring tethers either in the form of optical fibers or electrical wires to connect to a benchtop section.

Laser Speckle Contrast Imaging (LSCI) [17] is a specific imaging technique that enables extraction of relative blood flow information in both the spatial and temporal domains. Because orderly blood flow within vessels acts as a virtual contrasting agent LSCI is capable of producing images of vascular networks with higher contrast than traditional reflectance imaging [18]. Due to its wide-field and non-scanning nature [19], it has become a popular imaging modality in many research investigations including stroke [20] and migraine [21] research as well as retinal [22] and skin [23] imaging.

Miao *et al.* [24] reported a miniaturized LSCI setup capable of imaging in behaving animals. However, this head mounted imager system occupied a volume of $\sim 40\ \mathrm{cm}^3$ and weighed 20 g, while needing an external benchtop laser light source to be connected via a fiber bundle. In this paper, we expand our previous work [25], [26] on the design of a miniaturized laser speckle imaging microscope and image acquisition circuitry weighing only 7 g and occupying $\sim 5\ \mathrm{cm}^3$. Previously, our group designed an epi-illuminated microscope that can acquire reflectance images with LED light [27]. We altered this architecture to one that is capable of acquiring laser speckle images. Section II describes the optical analysis. A Monte Carlo simulation is used to estimate the depth visibility of the microscope while Fresnel diffraction integrals are calculated to analyse the speckle Airy disc pattern for the optical system. The speckle contrasting calculations are also described. Section III looks at the image acquisition and control circuitry. Section IV presents simulation and *in vivo* results while Section V discusses the uses and implications of our system for scientific research.

Manuscript received March 27, 2012; revised June 13, 2012; accepted July 19, 2012. Date of publication October 22, 2012; date of current version November 28, 2012. This work was supported by NIH grant R01AG029681. This paper was recommended by Associate Editor P. Hafliger.

J. Senarathna and N. Thakor are with the Department of Biomedical Engineering, Johns Hopkins University, Baltimore, MD 21205 USA (e-mail: dsenara1@jhu.edu).

K. Murari is with the Department of Electrical and Computer Engineering, University of Calgary, Calgary, AB T2N 1N4, Canada.

R. Etienne-Cummings is with the Department of Electrical and Computer Engineering, Johns Hopkins University, Baltimore, MD 21218 USA.

Color versions of one or more of the figures in this paper are available online at http://ieeexplore.ieee.org.

Digital Object Identifier 10.1109/TBCAS.2012.2218106

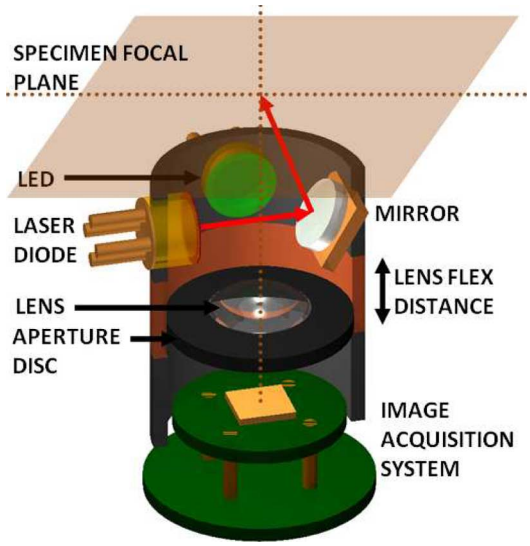

Fig. 1. A schematic of the LSCI microscope architecture.

II. Optical Design

The proposed microscope architecture is first described and then analysed using a Monte Carlo simulation and Fresnel diffraction.

A. Laser Speckle Microscope Architecture

We based our work on the epi-illuminated reflectance microscope designed by Murari *et al.* [27]. Utilizing our earlier design [25], we modified it to include production of laser speckles. This was reported in [26]. Briefly, a $f = 4.6$ mm (Thorlabs A390-A) lens is used achieving a magnification of ~ 0.75 within the 20 mm microscope tube. The architecture allowed for the lens to be moved along the tube axis for focusing purposes. Nonetheless, the lens was always positioned close to the specimen object plane for improving the magnification factor. The aperture radius is set at 190 μm. A tri-wavelength VCSEL (Vixar Inc, MN) in the red to near IR range (670 nm, 795 nm, 850 nm) is used as the laser source. The angle of illumination with the vertical is set between $30^0 \sim 40^0$. An additional wide angle green LED is used to provide illumination for focusing purposes (laser light is not suitable for this procedure as the speckles blur the image) at the time of initial microscope attachment. Fig. 1 shows a schematic of this set up.

B. Estimation of Depth Visualization Capacity Using a Monte Carlo Simulation

A Monte Carlo simulation model [28] incorporating the microscope architecture is devised for the purpose of estimating the microscope's ability to visualize information over a depth range. It consists of an angled illumination source, a semi-infinite biological tissue section with average absorption and scattering properties and the microscope aperture placement and dimensions for allowing light to pass through to the CMOS camera.

As scattering by biological tissue in the long wavelength range show only a weak relationship with wavelength [29], a nominal 1 mm^{-1} [30] is chosen as the scattering coefficient. Hemoglobin (oxy/deoxy) is considered the main absorbent in the biological tissue. An average Hemoglobin concentration of 80 μM with a typical blood oxygen saturation level of 70% is used [30]. These were used with the absorption properties of Hemoglobin [31] to arrive at the absorption coefficients $0.020\,\mathrm{mm}^{-1}$, $0.015\ \mathrm{mm}^{-1}$ and $0.0175\ \mathrm{mm}^{-1}$ at 670 nm, 795 nm and 850 nm, respectively. A Henyey-Greenstein scattering approximation with an anisotropy factor of 0.9 is used. A total of 100 million photons are used in each trial of the Monte Carlo simulation.

This model is used to estimate the effect of varying vertical angle of incident illumination on three specific parameters: the average maximum visible depth, the quartile depths and the uniformity in illumination. Average maximum visible depth calculates the expected value for the maximum depth travelled by a photon reaching the image sensor. The quartile depths consist of three separate distributions; first quartile depth (d_{Q1}), third quartile depth (d_{Q3}) and the inter-quartile depth range (d_{Q3-Q1}). First quartile depth is the average depth travelled by the shallowest 25% of photons reaching the image sensor, while the third quartile depth is the same for 75%. The inter-quartile depth range is the difference between these two depths, and gives a measure for the range of depths from which photons arrive to the camera. Finally, we calculated a measure of uniformity in illuminating the subject specimen, as visible to the camera $[U(\theta)]$. We define this as the ratio of the number of photons arriving at the image sensor from a unit length in the inter-quartile depth range to the number of photons arriving at the image sensor from a unit length in the first quartile depth. This is mathematically stated as

$$U(\theta) = \frac{\frac{0.5}{d_{Q3-Q1}}}{\frac{0.25}{d_{Q1}}} = \frac{2d_{Q1}}{d_{Q3-Q1}}. \tag{1}$$

The above calculation is done for the vertical depth axis. A $U(\theta)$ closer to unity will ensure a near uniform illumination profile for visible depth.

C. Analysis of Speckle Airy Disc Patterns for the Microscope

Size of laser speckles at the microscope imaging plane is governed by its Airy disc pattern. For a specific wavelength, this pattern depends on three major factors, namely: focal length of lens and object/image plane distances, dimensions of the aperture and the relative placement of aperture with respect to lens. The latter is often neglected in far field diffraction as it is sufficiently close to the lens plane.

Typically, the relationship, $d_{speckle} = 2.44\lambda(1+M)(f/D)$ where $d_{speckle}$ is the speckle diameter, λ is the wavelength of light, M is the magnification factor, f is the focal length of the lens and D is the diameter of the aperture [19], is used to calculate speckle diameter in the context of far-field diffraction. Specifically, with limited diffraction distance (from aperture plane to image plane) characteristic of our microscope, speckle patterns are more likely to be near-field and fluctuate largely with distance. Hence, using Fresnel integrals we simulated the diffraction pattern arising in a simplified model of our microscope architecture to investigate not only speckle size but also the overall speckle pattern developed at the image plane.

The simplified setup consists of a thin lens with $f = 4.6\,\mathrm{mm}$ positioned 10 mm above the specimen surface. An object plane 0.5 mm below the specimen surface is taken to be in focus with a nominal unity refractive index assumed for the biological media. (If needed, depths in the specimen can be scaled by the relative refractive index to arrive at more realistic estimates.). The imager is assumed to be placed in the image formation plane hence capturing the image at a magnification factor of 0.77 (This is in close agreement to the previously calibrated magnification value of 0.75). A nominal distance of 1 mm is assumed between the lens and the aperture planes. An aperture of 190 μm is used. An imagingary point light source placed along the optical axis in the object plane is used to generate the Airy disc pattern.

Fresnel diffraction arising from a circular aperture [32] was used. Equation (2) shows the diffracted electric field $U_{img}(x', y')$ observed in the imaging plane positioned at a distance z' away from the aperture plane (all scaling terms have been excluded for clarity).

$$U_{img}(x', y') = \frac{1}{\lambda}.\int_{S_{apt}} U_{apt}(x, y).exp\left[\frac{jk}{2z'}.r^2\right] dS \qquad (2)$$

where $r^2 = (x' - x)^2 + (y' - y)^2$.

$U_{apt}(x, y)$ is the radiation pattern illuminating the aperture plane. $k = 2\pi/\lambda$ is the wave number for wavelength λ. Essentially, $U_{apt}(x, y)$ depends on aperture sizing, as $U_{apt} = 0$ is assumed outside the aperture area.

Effect of wavefront convergence due to the lens as seen at the aperture is factored in by modifying the phase of $U_{apt}(x, y)$. Equation (2) was then cast as a two dimensional Fourier transform [33] and solved numerically. The calculated electric field magnitudes are squared to arrive at the final light intensity distributions constituting the Airy disc pattern. All calculations are done using MATLAB (Mathworks, MA) software.

D. Laser Speckle Contrasting Calculations

Speckle contrast at each pixel $k\,(x, y, t)$ is calculated as shown below in the temporal domain to preserve spatial resolution [34]

$$k\,(x, y, t) = \frac{\sigma_N}{\mu_N} \qquad (3)$$

where σ_N is the standard deviation and μ_N is the mean of pixel intensities within the neighbourhood N of each pixel. We used a N of 240 pixels in the time axis at every pixel location. The k value is related to the decorrelation time (τ_c) of blood flow by [35]

$$k^2 = \frac{\tau_c}{2T}.\left[2 - \frac{\tau_c}{T}\left\{1 - exp\left(\frac{-2T}{\tau_c}\right)\right\}\right] \qquad (4)$$

where T is the camera exposure time. τ_c is generally taken to be inversely related to the scatterer (red blood cell) average velocity [36]. Hence, normalized maps of $1/\tau_c$ are typically used to visualize relative distribution of spatial and temporal blood flow patterns within the region of interest.

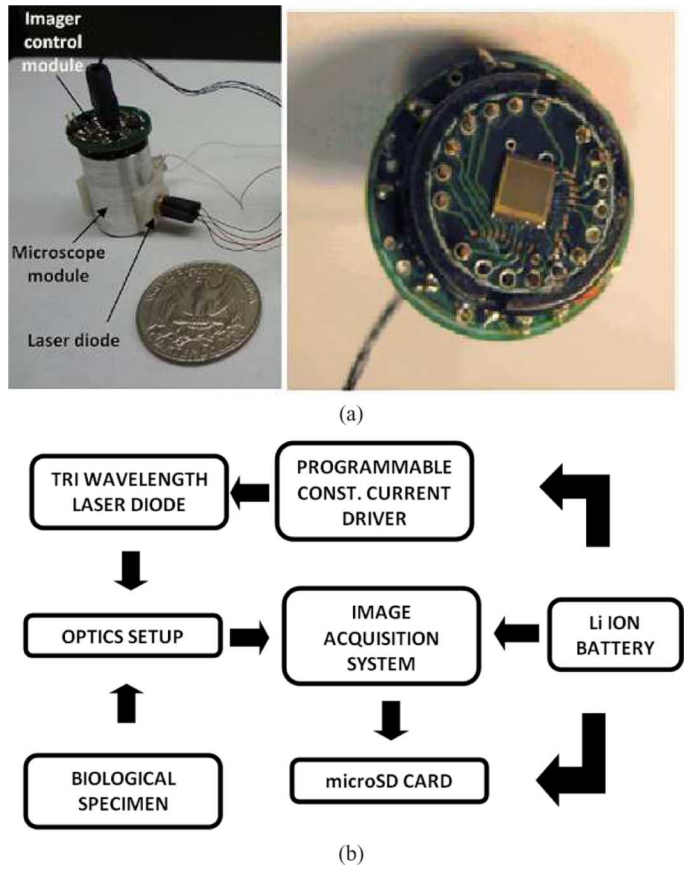

Fig. 2. Image acquisition and control circuitry. (a) The microscope — mounted image acquisition system. (b) A schematic of the overall system.

III. Image Acquisition and Control System

A custom designed CMOS imager chip of 132×124 pixels with performance comparable to a cooled CCD camera [37] is used to acquire the raw speckle images. The imager chip was previously characterized for fluorescent imaging [37] at 450 nm but has a broad spectrum ranging from 400 nm–900 nm. Table I summarizes its key features. A dedicated micro-controller (Microchip PIC24HJ32GP202) is used to control the image acquisition from the CMOS camera chip. This is mounted atop the microscope. Images are acquired at $\sim 6\,\mathrm{frames\ per\ second}$ with an inverse $(\sim 167\ \mathrm{ms})$ exposure time due to the rolling shutter nature of imager operation. Analog to digital conversion (ADC) at 12 bits resolution (reference 3.3 V) is done using the micro-controller ADC module. Fig. 2(a)(left) shows a picture of the image acquisition system mounted atop the microscope, while Fig. 2(a)(right) shows an enlarged view of the imager.

The digitized data are transferred to a 1 GB μSD card located in a back pack mounted on the rat. The laser driver is collocated in the backpack and sends its control currents to the microscope —mounted light sources. It consists of a separate microcontroller (Microchip PIC16LF1827) for programmable current values. The digital codes stored in the micro-controller are first converted to an analog voltage values using a 12 bit Digital to Analog converter module (Texas Instruments, DAC7574) and transformed to fixed current outputs via a voltage to current converter circuit. The constant currents are multiplexed between the

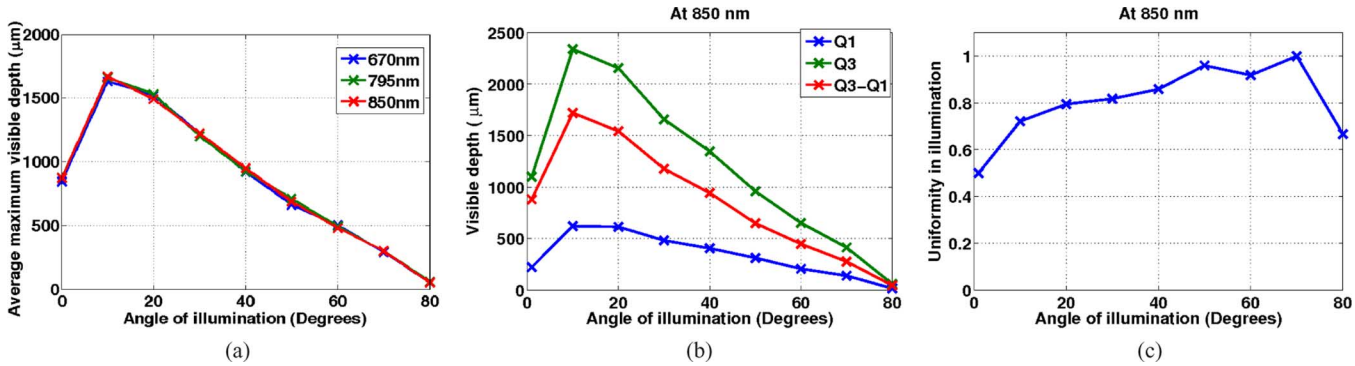

Fig. 3. Results from Monte Carlo simulations. The effect of angle of illumination on (a) the average maximum depth, (b) the quartile depth distributions at 850 nm, and (c) the uniformity in illumination at 850 nm.

TABLE I
IMAGER CHARACTERISTICS

Pixel count	132 x 124
Pixel size	20.1 μm x 20.1 μm
Fill factor	57.7%
CMOS technology	0.5 μm
Dark frame fixed pattern noise	0.99 %
Reported detection limit	
SNR	0 dB
Wavelength	450 nm
Exposure time	14.3 ms (70 fps)
Intensity	4 nW/ cm^2
Photon count	5.2 x 10^2

three laser wavelengths and the LED light source using a low resistance analog multiplexer (Analog Devices, ADG1404). The entire system was powered by a 3.7 V Li-ion battery. Fig. 2(b) shows a schematic block diagram of the entire system.

The microscope stage together with the image acquisition system weighs ~ 7 g, while the backpack module weighs ~ 22 g which is an acceptable weight for a rat to carry. The overall system consumes ~ 40 mA which is roughly divided as 30 mA and 10 mA amongst the laser driver and the imager controller circuitry/μSD card, respectively.

IV. RESULTS

We report the results from our simulations as well as *in vivo* studies. All animal procedures were first approved by the Johns Hopkins Animal Care and Use Committee (ACUC).

A. Monte-Carlo Simulations

Fig. 3(a)–(c) shows the results of the Monte Carlo simulation. As indicated by Fig. 3(a), the visible depth profiles for all three wavelengths 670 nm, 795 nm and 850 nm are approximately the same, owing to the similarity in their absorption coefficients (0.015, 0.020 and 0.0175 mm^{-1}). Furthermore, it shows that at an angle of $30^{\,0} \sim 40^{\,0}$, the microscope is able to capture an average maximum depth in the order of 1 mm, which is considered satisfactory for imaging cortical surface vasculature.

Due to similarity of results shown in Fig. 3(a) and the fact that the absorption coefficient of 850 nm (0.0175 mm^{-1}) lies in between that of 670 nm (0.015 mm^{-1}) and 795 nm (0.020 mm^{-1}), data from simulations at 850 nm were used to further analyse the results. Fig. 3(b) shows the quartile distributions of visible depths for 850 nm. As shown, the system registers a third quartile depth (Q_3) in the range of 1–2 mm in the initial incident angle range $(<50^0)$. Additionally, the inter-quartile depth $(Q_3 - Q_1)$ itself accounts for more than ~ 1 mm in visible depth, for angles $<40^0$.

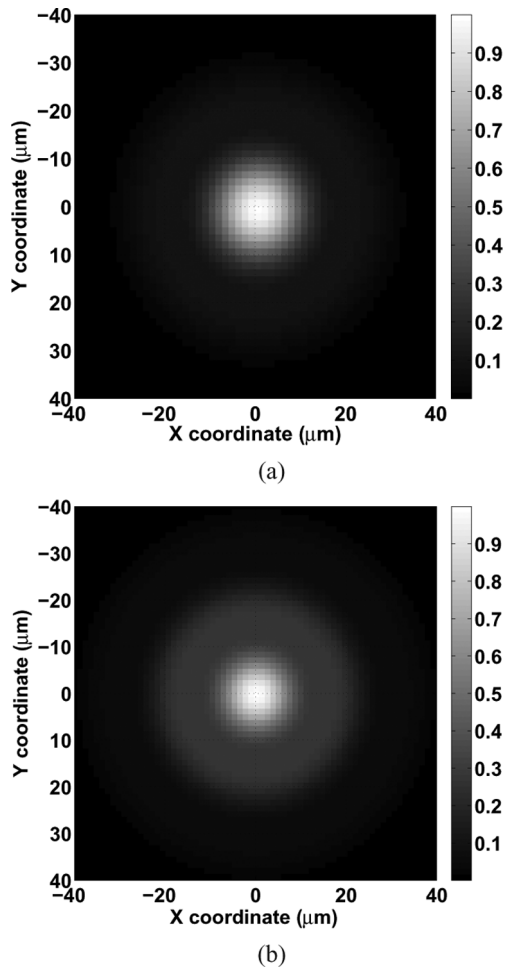

Fig. 4. The estimated effect of focus on the speckle pattern at 795 nm. (a) Object plane 0.5 mm above the plane of focus (i.e., estimated to be the specimen surface) and (b) object plane 2 mm deeper than the in focus plane. A plane 0.5 mm below the specimen surface was taken as the in focus plane.

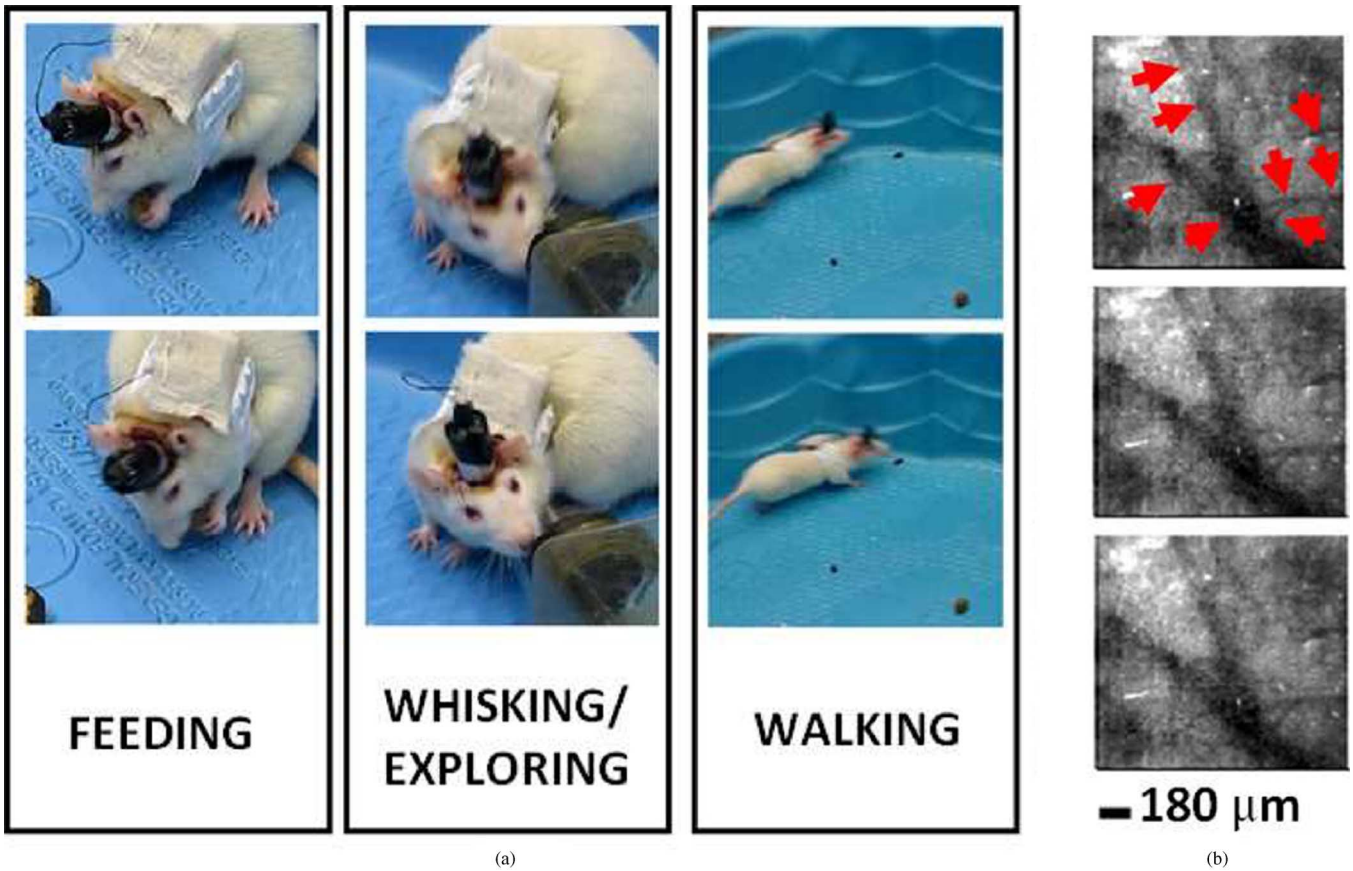

Fig. 5. Results of behavioral experiment. (a) Instances of the rat behaving naturally with the microscope mounted on its head. (b) Corresponding images while the rat is walking. (The image indented with red arrows is a baseline image acquire while the rat was anesthetized, and is shown for comparison. The reflectance images are contrast enhanced for the purpose of better visualizing the vasculature. The arrows indicate blood vessels.)

Finally, the uniformity of illumination, as shown in Fig. 3(c), is kept at a consistently high level. Specifically, a value of $\sim 85\%$ at an incident angle of 40^0 suggests that the proposed architecture is fairly suitable of observing details through out the depth profile of interest (~ 1 mm) with satisfactory uniform illumination.

B. Speckle Airy Disc Simulations

A Fresnel diffraction simulation is used to analyze the fluctuation in speckle Airy disc pattern for a set of control parameters. We previously reported that the speckle pattern remains adequately robust for the wavelength range of interest (670 nm–850 nm) [26]. Here we show its variation due to object plane being out of focus. It is important that the speckle Airy disc patterns remain insensitive to depth variations in order to capture information from a larger depth range.

Fig. 4 shows how the speckle Airy disc pattern varied between two extreme instances at 795 nm. Fig. 4(a) shows the speckle Airy disc pattern for purely superficial objects and Fig. 4(b) shows the same for an object plane 2 mm below the in focus plane. These results suggest that the speckle Airy disc patterns remains within a range of 30 μm–50 μm range. Hence, they are estimated to be satisfactorily robust to variations in depth thus being able to capture information from a range of depths. These model based estimates were used as justification for choosing an aperture radius of 190 μm, the major control variable responsible for the speckle Airy disc patterns. Nonetheless, the quality of actual speckles produced has to be judged by the standard of the final speckle contrasted images.

C. Testing On Awake Animal

We tested the system components on an awake rat model. Two concerns were addressed. First, the impact of the surgically head mounted microscope on an awake rat's behavior was monitored. Secondly, the ability of the image acquisition system to capture information over a period of time was ascertained. This was of considerable interest because the thinned skull preparation is known to deteriorate in transparency over time. As the LSCI setup was still to be validated, normal green reflectance images were acquired by our earlier base design [27]. The animal preparation was done as reported earlier [27] and the animal allowed to wake up from anesthesia. Fig. 5 shows several results.

As shown in Fig. 5(a), the animal appeared to perform its normal habitual tasks without noticeable anomalies. Hence, we ascertained that the surgically head mounted microscope system does not cause any unwanted impact on the animal's behavior. Furthermore, Fig. 5(b) shows several images of the acquired image stack. The top image with blood vessels marked corresponds to while the rat was still anesthetized and the bottom two images were acquired when the rat was walking. These

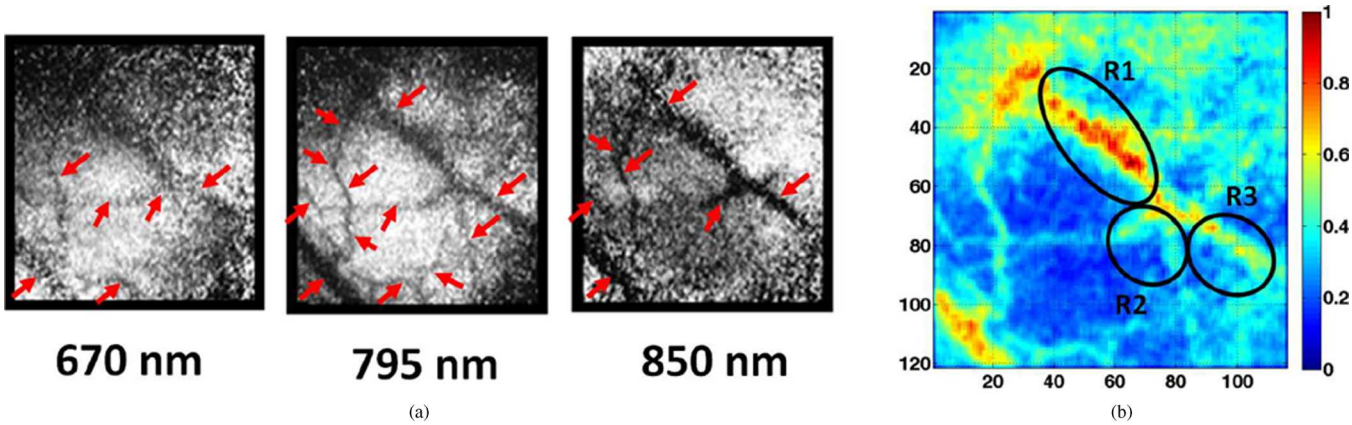

(a) (b)

Fig. 6. Laser speckle contrast image data. (a) Speckle contrasted images at 670 nm, 795 nm, and 850 nm showing the structural details of vasculature for an area of $\sim 1.85\ \mathrm{mm} \times 2.0\ \mathrm{mm}$. The arrows indicate visible blood vessels. (b) Normalized $1/\tau_c$ map of the 795 nm speckle contrasted image. Prior to normalization the flow map was smoothed by a 3×3 window. Regions $R1$, $R2$ and $R3$ are annotated for analysis purposes. 240 frames acquired over ~ 40 s were used for each calculation.

were captured after ~ 1 hours post microscope implantation. We noted that the image quality does marginally degrade over time, but is within satisfactory limits for our purposes.

D. Laser Speckle Contrast Analysis

For this experiment, data were recorded directly from the imager control circuitry for real time analysis (The backpack system was not used as the experiment was on an anesthetized animal and as it would not provide real time data visualization). Images at the three different laser wavelength were acquired sequentially. Fig. 6 shows several results of laser speckle contrasted images captured over a period of ~ 40 s. 240 raw speckle images were used to construct each contrasted image.

As shown in Fig. 6(a), 795 nm produced the best visible vascular details out of the three wavelengths utilized. The variations should not be interpreted as an absolute relationship between flow characteristics and speckle contrasts at different wavelengths, but rather as a manifestation of several factors such as the imaging geometry and the imperfections in the illumination source etc. Hence, the ability to utilize multiple wavelengths provided an additional means of flexibility to fine tune the system for better information acquisition. Fig. 6(b) shows the smoothed normalized $1/\tau_c$ map for the 795 nm laser speckle image. This essentially provides a spatial map of relative blood flow in the region of interest. For example, it can be clearly seen that the flow level in the annotated region $R1$ is greater than the individual flow levels in regions $R2$ and $R3$. It can thus be concluded that blood is flowing from region $R1$ and branching off into the vessels in regions $R2$ and $R3$. Such insights highlight the validity of our system in providing hemodynamic information beyond mere structural details.

V. Discussion

We have described the construction of a miniaturized laser speckle imaging microscope system. LSCI can be used to explore superficial hemodynamic patterns with good spatial and temporal resolution. Theoretically, the spatial resolution is limited by the speckle Airy disc size which needs to be matched to twice the pixel size [38] owing to the Nyquist criterion. This ensures a good signal to noise ratio. Nonetheless, many previous studies [34], [39] have used a 1:1 match between pixels and speckle size while still producing quality speckle contrasted images. On the other hand, temporal resolution depends largely on the frame rate and the speckle contrasting neighborhood used. Accordingly, it can vary from several tens of milli-seconds to several seconds. Thus, LSCI can be tailored for dynamic [40], [41] or structural imaging [42], [43].

The utility of LSCI is enhanced due to its simple nature which allows it to be used in conjunction with other techniques such as multi-spectral reflectance imaging [39] and fluorescence imaging [44]. Furthermore, LSCI has found great use in longitudinal angiogenic studies over several weeks [45]. Hence, our miniaturized LSCI microscope system could enable a multitude of experimental studies to be performed on behaving rodents.

We overcame several challenges in the process of miniaturization while compromises were made in others. Designing an optical system within a small foot-print but still producing quality speckles was one. Fresnel diffraction simulations were used to estimate the speckle Airy disc patterns and decide on a practical aperture size. The angle of incident illumination had to be considerably slant in order to keep the microscope dimensions small. This posed the question whether an appropriate level of depth is illuminated. The Monte Carlo simulation enabled a better understanding of this situation. The miniature red to IR range VCSEL (Vixar Inc, MN) provided a means of miniaturizing the illumination source, thus preventing the necessity to draw optical fibers from a benchtop laser source. Furthermore, the use of a highly sensitive CMOS imager chip [37] eradicated the need for optical signals to be transferred to a benchtop cooled CCD camera. Additionally, the microscope attachment mechanism detailed in [46] allowed for a strong contact with the skull, minimizing possible motion artifacts. No significant motion artifacts were observed in the reflectance images acquired during the behaving animal experiment. However, as the LSCI technique was demonstrated on an anesthetized rat, it is yet to be confirmed whether motion artifacts play a role in unduly blurring the laser speckle images. Use of

registered laser speckle contrast analysis [47] that re-aligns raw speckle images to counteract motion artifacts can be utilized in such an event to improve the speckle contrast calculations.

On the other hand, due to the low frame rate of our imaging system (~ 6 fps resulting because the microcontroller is handling both ADC and digital transmission to μSD card), it has a large exposure time of ~ 167 ms. A long exposure time averages out the speckle variations unnecessarily and impairs speckle contrast. Hence, the contrasted images displayed high noise levels. As a result, 240 raw speckle images instead of a typical amount of 80 [43] raw images were used to create our speckle contrast image. Hence the problem of low frame rate compounds with the necessity for a higher frame count per single speckle contrast image calculation and results in a very low temporal resolution of 40 s. Thus, the LSCI technique was used to study the vascular structure in an anesthetized rat model. Nonetheless, the exposure time needs to be lowered for higher quality image formation. Utilizing a high speed ADC system capable of sampling images in the range of 2 MS/s will allow for exposure times in the range of 10 ms, which is more closer to the standard 5 ms exposure time used commonly. Furthermore, the resolution was limited to 12 bits because we used the ADC module of the micro-controller. A dedicated 16 bit ADC chip will be a solution worthwhile pursuing. Additionally, use of anisotropy in speckle contrast neighborhood selection by taking additional pixels along the axis of the blood vessel for speckle contrast calculation, can be used to reduced the number of separate frames needed while effectively preserving the spatial resolution [48]. Lack of a fine focusing mechanism was another constraint imposed by the current design which can be improved by sophisticated mechanical design. The large current consumption (~ 30 mA) by the laser driver circuit is mainly due to the use of a multiple operational amplifier based voltage to current converter circuit, whereas the laser diode only consumes under 3 mA. While low current level through the laser diode allows it to be safely operated without significant heating concerns, using a current mirror chip such as ADL5315 (Analog Devices, MA) instead to drive the light source can considerably reduce the overhead current consumption. The microscope system was separately tested on an awake animal model while its speckle capabilities were demonstrated only on an anesthetized rat. We intend to test our LSCI system for monitoring functional hemodynamic changes on an acute behaving animal model once the above limitations are addressed. Chronic experiments in the order of weeks are envis with the use of a polished glass window instead of a thinned skull preparation.

VI. Conclusion

We report the design details of a miniaturized microscope architecture and supporting control circuitry for acquiring laser speckle images. The new architecture is analysed using both Monte Carlo simulations for its depth visualization capacity and Fresnel integral simulations for its diffraction properties. The microscope structure is thus estimated to visualize information within a 1 mm depth range with approximate uniform illumination as well as produce speckles in the order of 30 μm to 50 μm in the wavelength range 670 nm to 850 nm. Details of the image acquisition and control circuitry is presented. The microscope and image acquisition system is then tested for its ability to capture data in an awake animal model. Finally, we report results of laser speckle contrasted images and relative blood flow showing proof of concept for the miniaturized microscope design.

Acknowledgment

The authors would like to thank J. Burns at the JHU BME Machine shop for helping with the microscope construction and Dr. N. Li for helping with experiments.

References

[1] B. Winegar and M. MacIver, "Isoflurane depresses hippocampal ca1 glutamate nerve terminals without inhibiting fiber volleys," *BMC Neurosci.*, vol. 7, no. 5, 2006.

[2] J. Berg-Johnsen and I. Langmoen, "The effect of isoflurane on excitatory synaptic transmission in the rat hippocampus," *Acta. Anaesthesiol. Scand.*, vol. 36, no. 4, pp. 350–355, 1992.

[3] I. Ferezou, S. Bolea, and C. Petersen, "Visualizing the cortical representation of whisker touch: Voltage-sensitive dye imaging in freely moving mice," *Neuron*, vol. 50, no. 4, pp. 617–629, 2006.

[4] D. Ng, H. Tamura, T. Tokuda, A. Yamamoto, M. Matsuo, and M. Nunoshita, "Real time in vivo imaging and measurement of serine protease activity in the mouse hippocampus using a dedicated complimentary metal-oxide semiconductor imaging device," *J. Neurosci. Methods*, vol. 156, no. 1–2, pp. 23–30, 2006.

[5] H. Tamura, D. Ng, T. Tokuda, H. Naoki, T. Nakagawa, T. Mizuno, Y. Hatanaka, Y. Ishikawa, J. Ohta, and S. Shiosaka, "One-chip sensing device (biomedical photonic lsi) enabled to assess hippocampal steep and gradual up-regulated proteolytic activities," *J. Neurosci. Methods*, vol. 173, no. 1, pp. 114–120, 2008.

[6] J. Ohta, A. Higuchi, A. Tagawa, K. Sasagawa, T. Tokuda, Y. Hatanaka, H. Tamura, and S. Shiosaka, "An implantable cmos image sensor for monitoring deep brain activities of a freely moving mouse," in *Proc. IEEE Biomed. Circuits and Systems Conf.*, 2008, pp. 269–272.

[7] B. Flusberg, A. Nimmerjahn, E. Cocker, E. Mukamel, R. Barretto, T. Ko, L. Burns, J. Jung, and M. Schnitzer, "High-speed, miniaturized fluorescence microscopy in freely moving mice," *Nature Methods*, vol. 5, no. 11, pp. 935–938, 2008.

[8] K. K. Ghosh, L. D. Burns, E. D. Cocker, A. Nimmerjahn, Y. Ziv, A. E. Gamal, and M. J. Schnitzer, "Miniaturized integration of a fluorescence microscope," *Nature Methods*, vol. 8, pp. 871–878, 2011.

[9] T. Kobayashi, H. Tamura, Y. Hatanaka, M. Motoyama, T. Noda, K. Sasagawa, T. Tokuda, Y. Ishikawa, S. Shiosaka, and J. Ohta, "Functional neuroimaging by using an implantable cmos multimodal device in a freely-moving mouse," in *Proc. IEEE Biomed. Circuits and Systems Conf.*, 2011, pp. 110–113.

[10] J. Park, V. Pieribone, and E. Culurciello, "Miniature voltage sensitive dye imaging system for in vivo imaging," in *Proc. IEEE Life Science Systems and Applications Workshop*, 2009, pp. 70–73.

[11] J. H. Park, J. Platisa, J. V. Verhagen, S. H. Gautamb, A. Osman, D. Kima, V. A. Pieribone, and E. Culurciello, "Head-mountable high speed camera for optical neural recording," *J. Neurosci. Methods*, vol. 201, no. 2, pp. 290–295, 2011.

[12] A. Osman, J. Park, D. Dickensheets, J. Platisa, E. Culurciello, and V. Pieribone, "A head-mountable microscope for high-speed fluorescence brain imaging," in *Proc. Biomed. Circuits and Systems Conf.*, 2011, pp. 114–116.

[13] Y. Sabharwal, A. Rouse, L. Donaldson, M. Hopkins, and A. Gmitro, "Slit-scanning confocal microendoscope for high-resolution in vivo imaging," *Appl. Opt.*, vol. 38, pp. 7133–7144, 1999.

[14] C. Engelbrecht, R. Johnston, E. Seibel, and F. Helmchen, "Ultracompact fiber-optic two-photon microscope for functional fluorescence imaging in vivo," *Opt. Express*, vol. 16, no. 8, pp. 5556–5564, 2008.

[15] D. Dombeck, A. Khabbaz, F. Collman, T. Adelman, and D. Tank, "Imaging large-scale neural activity with cellular resolution in awake, mobile mice," *Neuron*, vol. 56, no. 1, pp. 43–57, 2007.

[16] D. Schulz, S. Southekal, S. S Junnarkar, J.-F. Pratte, M L. Purschke, S. P. Stoll, B. Ravindranath, S. H. Maramraju, S. Krishnamoorthy, F. A. Henn, P. O'Connor, C. L. Woody, D. J. Schlyer, and P. Vaska, "Simultaneous assessment of rodent behavior and neurochemistry using a miniature positron emission tomograph," *Nature Methods*, vol. 8, no. 4, pp. 347–354, 2011.
[17] A. Fercher and J. Briers, "Flow visualization by means of single-exposure speckle photography," *Opt. Commun.*, vol. 37, no. 5, pp. 326–330, 1981.
[18] K. Murari, N. Li, A. Rege, X. Jia, A. All, and N. Thakor, "Contrast-enhanced imaging of cerebral vasculature with laser speckle," *Appl. Opt.*, vol. 46, no. 22, pp. 5340–5346, 2007.
[19] D. A. Boas and A. K. Dunn, "Laser speckle contrast imaging in biomedical optics," *J. Biomed. Opt.*, vol. 15, no. 1, pp. 011109–011109, 2010.
[20] Z. Luo, Z. Yuan, Y. Pan, and C. Du, "Simultaneous imaging of cortical hemodynamics and blood oxygenation change during cerebral ischemia using dual-wavelength laser speckle contrast imaging," *Opt. Lett.*, vol. 34, no. 9, pp. 1480–1482, 2009.
[21] N. Li, X. Jia, K. Murari, R. Parlapalli, A. Rege, and N. V. Thakor, "High spatiotemporal resolution imaging of the neurovascular response to electrical stimulation of rat peripheral trigeminal nerve as revealed by in vivo temporal laser speckle contrast," *J. Neurosci. Methods*, vol. 176, no. 2, pp. 230–236, 2009.
[22] L. Winchester and N. Chou, "Measurement of retinal blood velocity," in *Proc. SPIE 16th Ophthalmic Technologies*, 2006, vol. 6138, pp. 383–390.
[23] V. Kalchenko, D. Preise, M. Bayewitch, I. Fine, K. Burd, and A. Harmelin, "In vivo dynamic light scattering microscopy of tumour blood vessels," *J. Microsc.*, vol. 228, no. Pt 2, pp. 118–122, 2007.
[24] P. Miao, S. Tong, H. Lu, Q. Liu, and Y. Li, "Laser speckle contrast imaging of cerebral blood flow in freely moving animals," *J. Biomed. Opt.*, vol. 16, no. 9, pp. 090502–090502, 2011.
[25] J. Senarathna, K. Murari, N. Li, R. Etienne-Cummings, and N. Thakor, "Miniaturized laser speckle contrast imaging microscope," in *Proc. Math. and Comp. Biomed. Eng. Conf.*, 2011, pp. 301–304.
[26] J. Senarathna, K. Murari, R. Etienne-Cummings, and N. V. Thakor, "Design of a novel head-mountable microscope system for laser speckle imaging," in *Proc. IEEE Biomed Circuits and Systems Conf.*, 2011, pp. 117–120.
[27] K. Murari, R. Etienne-Cummings, G. Cauwenberghs, and N. Thakor, "An integrated imaging microscope for untethered cortical imaging in freely-moving animals," in *Proc. IEEE Eng. Med. Biol. Soc. Conf.*, 2010, pp. 5795–5798.
[28] L. Wang, S. Jacques, and L. Zheng, "Mcml—Monte carlo modelling of light transport in multi-layered tissues," *Comput. Methods Programs Biomed.*, vol. 47, no. 2, pp. 131–146.
[29] Near-Infrared Spectroscopy for the Study of Biological Tissue, T. U. Sergio Fantini's Group, Department of Biomedical Engineering [Online]. Available: http://ase.tufts.edu/biomedical/research/fantini/researchAreas/NearInfraredSpectroscopy.pdf
[30] M. Kohl, U. Lindauer, G. Royl, M. Kuhl, L. Gold, A. Villringer, and U. Dirnagl, "Physical model for the spectroscopic analysis of cortical intrinsic optical signals," *J. Phys. Med. Biol.*, vol. 45, no. 12, pp. 3749–3764, 2000.
[31] S. Prahl, Tabulated Molar Extinction Coefficient for Hemoglobin in Water, 1998 [Online]. Available: http://omlc.ogi.edu/spectra/hemoglobin/summary.html
[32] R. Sheppard and M. Hrynevych, "Diffraction by a circular aperture: A generalization of fresnel diffraction theory," *J. Opt. Soc. Amer. A.*, vol. 9, no. 2, pp. 274–281, 1992.
[33] J. Goodman, *Introduction to Fourier Optics*, 3rd ed. Greenwood Village, CO: Roberts, 2005.
[34] H. Cheng, Q. Luo, S. Zeng, S. Chen, J. Cen, and H. Gong, "Modified laser speckle imaging method with improved spatial resolution," *J. Biomed. Opt.*, vol. 8, no. 3, pp. 559–564, 2003.
[35] D. D. Duncan and S. J. Kirkpatrick, "Can laser speckle flowmetry be made a quantitative tool?," *J. Opt. Soc. Amer. A, Opt. Image Sci. Vis.*, vol. 25, no. 8, pp. 2088–2094, 2008.
[36] J. D. Briers and S. Webster, "Laser speckle contrast analysis (lasca): A nonscanning, full-field technique for monitoring capillary blood flow," *J. Biomed. Opt.*, vol. 1, no. 2, pp. 174–179, 1996.
[37] K. Murari, R. Etienne-Cummings, N. Thakor, and G. Cauwenberghs, "A cmos in-pixel ctia high sensitivity fluorescence imager," *IEEE Trans. Biomed. Circuits Syst.*, vol. 5, no. 5, pp. 449–458, 2011.
[38] S. J. Kirkpatrick, D. D. Duncan, and E. M. Wells-Gray, "Detrimental effects of speckle-pixel size matching in laser speckle contrast imaging," *Opt. Lett.*, vol. 33, no. 24, pp. 2886–2888, 2008.
[39] A. K. Dunn, A. Devor, A. M. Dale, and D. A. Boas, "Spatial extent of oxygen metabolism and hemodynamic changes during functional activation of the rat somatosensory cortex," *Neuroimage*, vol. 27, no. 2, pp. 279–290, 2005.
[40] A. J. Strong, E. L. Bezzina, P. J. Anderson, M. G. Boutelle, S. E. Hopwood, and A. K. Dunn, "Evaluation of laser speckle flowmetry for imaging cortical perfusion in experimental stroke studies: Quantitation of perfusion and detection of peri-infarct depolarisations," *J. Cereb. Blood Flow Metab.*, vol. 26, no. 5, pp. 645–653, 2006.
[41] J. P. Dreier, J. Woitzik, M. Fabricius, R. Bhatia, S. Major, C. Drenckhahn, T.-N. Lehmann, A. Sarrafzadeh, L. Willumsen, J. A. Hartings, O. W. Sakowitz, J. H. Seemann, A. Thieme, M. Lauritzen, and A. J. Strong, "Delayed ischaemic neurological deficits after subarachnoid haemorrhage are associated with clusters of spreading depolarizations," *Brain*, vol. 129, no. Pt 12, pp. 3224–3237, 2006.
[42] P. Li, S. Ni, L. Zhang, S. Zeng, and Q. Luo, "Imaging cerebral blood flow through the intact rat skull with temporal laser speckle imaging," *Opt. Lett.*, vol. 31, no. 12, pp. 1824–1826, 2006.
[43] A. Rege, K. Murari, N. Li, and N. Thakor, "Imaging microvascular flow characteristics using laser speckle contrast imaging," in *Proc. IEEE Eng. Med. Biol. Soc. Conf.*, 2010, pp. 1978–1981.
[44] S. Sakadzic, S. Yuan, E. Dilekoz, S. Ruvinskaya, S. A. Vinogradov, C. Ayata, and D. A. Boas, "Simultaneous imaging of cerebral partial pressure of oxygen and blood flow during functional activation and cortical spreading depression," *Appl. Opt.*, vol. 48, no. 10, pp. D169–D177, 2009.
[45] A. Rege, N. V. Thakor, K. Rhie, and A. P. Pathak, "In vivo laser speckle imaging reveals microvascular remodeling and hemodynamic changes during wound healing angiogenesis," *Angiogenesis*, vol. 15, no. 1, pp. 87–98, 2012.
[46] K. Murari, "Optical Methods and Integrated Systems for Brain Imaging in Awake, Untethered Animals," Ph.D. dissertation, Dept. Biomedical Engineering, Johns Hopkins Univ., Baltimore, MD, 2010.
[47] P. Miao, A. Rege, N. Li, N. V. Thakor, and S. Tong, "High resolution cerebral blood flow imaging by registered laser speckle contrast analysis," *IEEE Trans. Biomed. Eng.*, vol. 57, no. 5, pp. 1152–1157, 2009.
[48] A. Rege, J. Senarathna, N. Li, and N. V. Thakor, "Anisotropic processing of laser speckle images improves spatiotemporal resolution," *IEEE Trans Biomed. Eng.*, vol. 59, no. 5, pp. 1272–1280, 2012.

Janaka Senarathna (S'11) received the B.Sc. degree in electronics and telecommunications engineering from the University of Moratuwa, Moratuwa, Sri Lanka, in 2008. He is currently working toward the M.S.E. degree in biomedical engineering at Johns Hopkins University, Baltimore, MD.

His current research interests include laser speckle contrast imaging and its miniaturization for behavioral studies.

Kartikeya Murari (S'02–M'10) received the B.Tech. degree in electrical engineering from the Indian Institute of Technology, Madras, India, in 2002, the M.S.E. degree in biomedical engineering from the Johns Hopkins University, Baltimore, MD, in 2004, and the Ph.D. degree in biomedical engineering from the Johns Hopkins University School of Medicine, Baltimore, in 2010.

He trained as a Postdoctoral Fellow at the Johns Hopkins University School of Medicine from 2010–2011. Currently, he is an Assistant Professor and an iCORE-ISIS Associate in the Department of Electrical and Computer Engineering at the University of Calgary, Canada. His research interests lie in mixed-signal very-large-scale integrated systems for biomedical applications in imaging, sensing, and power management and in optical imaging and imaging systems.

Ralph Etienne-Cummings (S'94–M'98–SM'08–F'12) received the B.Sc. degree in physics from Lincoln University, Oxford, PA, in 1988, and the M.S.E.E. and Ph.D. degrees in electrical engineering from the University of Pennsylvania, Philadelphia, in 1991 and 1994, respectively.

Currently, he is a Professor of electrical and computer engineering, and computer science at The Johns Hopkins University (JHU), Baltimore, MD. He is the former Director of Computer Engineering at JHU and the Institute of Neuromorphic Engineering, currently administered by the University of Maryland, College Park. He is also an Associate Director for Education and Outreach of the National Science Foundation (NSF) sponsored Engineering Research Centers on Computer Integrated Surgical Systems and Technology at JHU. His current research interests include mixed-signal very large scale integration systems, computational sensors, computer vision, neuromorphic engineering, smart structures, mobile robotics, legged locomotion, and neuroprosthetic devices.

Dr. Etienne-Cummings is the recipient of the NSF CAREER Award and the Office of Naval Research Young Investigator Program Award. In 2006, he was named a Visiting African Fellow and a Fulbright Fellowship Grantee for his sabbatical at the University of Cape Town, Rondebosch, South Africa. He was invited to be a Lecturer at the National Academies of Science Kavli Frontiers Program, held in 2007.

Nitish V. Thakor (S'78–M'81–SM'89–F'94) received the B.Tech. degree in electrical engineering from Indian Institute of Technology (IIT) Bombay, Mumbai, India, in 1974, and the Ph.D. degree in electrical and computer engineering from the University of Wisconsin, Madison, in 1981.

He is currently a Professor of Biomedical Engineering, Electrical Engineering and Neurology at Johns Hopkins University and directs the Laboratory for Neuroengineering. His technical expertise is in the areas of brain machine interface, neural prosthesis, diagnostic instrumentation, microsystems, signal processing, optical imaging of the brain and fundamental neuroscience research on injury, repair and recovery of the nervous system. He has published more than 200 refereed journal papers and generated 11 patents and carries out research funded mainly by the NIH, NSF and DARPA. He is the Director of a Neuroengineering Training program funded by the National Institute of Health. He is the Editor in Chief of IEEE Transactions on Neural and Rehabilitation Engineering and also the 2010 recipient of IEEE EMBS Technical Achievement Award in the field of Neuroengineering.

Dr. Thakor has received a Research Career Development Award from the National Institutes of Health and a Presidential Young Investigator Award from the National Science Foundation, and is a Fellow of the American Institute of Medical and Biological Engineering, IEEE and Founding Fellowof the Biomedical Engineering Society.